The 2026 International Power Electronics Conference (IPEC-Nagasaki 2026 -ECCE Asia-)

# Simplified Soft-Switching Constraints for High-Power Multi-Active Bridge Converters

Jonghun Yun
*Institute for Technical Physics (ITEP)*
*Karlsruhe Institute of Technology (KIT)*
Karlsruhe, Germany
jonghun.yun@kit.edu

Jaekeun Lee
*Department of Electrical and Computer Engineering*
*Seoul National University*
Seoul, Republic of Korea
jaek709@snu.ac.kr

Giovanni De Carne
*Institute for Technical Physics (ITEP)*
*Karlsruhe Institute of Technology (KIT)*
Karlsruhe, Germany
giovanni.carne@kit.edu

Shenghui Cui
*Department of Electrical and Computer Engineering*
*Seoul National University*
Seoul, Republic of Korea
cuish@snu.ac.kr

***Abstract*—A multi-active bridge (MAB) dc-dc converter, utilizing its multi-winding transformer, enables flexible power flow between multiple dc sources with minimized system components and power conversion stages. However, when voltage ratios among the multiple dc sources are mismatched, the efficiency deteriorates due to limited soft switching capability and increased reactive currents. Therefore, numerous modulation schemes have been developed, but the extensive degrees of freedom in duty cycle and phase-shift adjustments complicate their design. For simplicity, straightforward sufficient conditions have been used in some modulation designs to achieve soft-switching and compress the degrees of freedom to unity. However, these simplified soft-switching constraints have mainly been applied to single-phase MAB converters and not been fully addressed for three-phase MABs, which are emerging for high-power applications. This article extends these simplified soft-switching constraints from single-phase to three-phase MABs. Flux-domain analysis is presented to utilize the key principles of the single-phase MAB constraints and to adapt them for the three-phase configuration. The validity of the extended soft-switching constraints is demonstrated through experimental results.**

***Index Terms*—Multi-active bridge (MAB) converter, duty cycle control, soft-switching, modulation.**

## I. Introduction

In response to growing demand for dc sources in power systems, multi-active bridge (MAB) converters have become attractive [1]–[6]. The MAB converter is an extended topology of the dual-active bridge (DAB), using a multi-winding transformer. Compared to using multiple DAB converters, it enables flexible power flow control between multiple dc sources with higher power density and efficiency.

A multi-winding transformer in an MAB can be implemented with a single-phase or three-phase configuration. For high-power applications, the three-phase configuration offers advantages over the single-phase counterpart. Like the three-phase DAB over the single-phase DAB [7]–[10], the three-phase configuration can substantially reduce the volume of dc-link capacitors and transformers in MABs, while also lowering the switching losses [11]–[13].

For both single- and three-phase MABs, single phase-shift (SPS) modulation is currently the most widely adopted method for power flow control of MAB3 converters due to its simplicity and inherent soft-switching capability [14]–[16]. The SPS modulation adjusts only the load angles between multiple ports while maintaining duty cycles at one-half, thereby maximizing the applied voltages to the transformer. Due to these fixed duty cycles, when the dc voltages are mismatched among the ports, the soft-switching capability becomes limited, and the reactive currents are increased, leading to further degradation of efficiency, especially under light-load conditions.

To address these limitations of the SPS, multi-variable modulation schemes with adjustable duty cycles can be employed for MAB converters. By adjusting duty cycles to compensate for mismatched voltage ratios, these schemes can enhance light-load efficiency of not only single-phase MABs [17]–[21], but also three-phase MABs [12], [22]. However, the excessive degrees of freedom in multi-variable modulation induce significant complexity in modulation design. As the port number increases, the size of the candidate domain, consisting of duty cycles and load angles, increases exponentially.

To resolve this design complexity, some works have attempted to compress the degrees of freedom [23], [24]. The sufficient conditions to achieve soft-switching of single-phase MAB can be used to mathematically relate the duty cycles to each other. Therefore, if one of the duty cycles is determined, the other duty cycles are automatically determined, leading to simplifying modulation design . However, these soft switching constraints for single-phase MABs are not directly applicable

This work was supported in part by the Korea Institute of Energy Technology Evaluation and Planning, Korea Government (MCEE), under Grant 20224000000160 (DC Grid Energy Innovation Research Center), and in part by the Helmholtz Association under the program "Energy System Design."

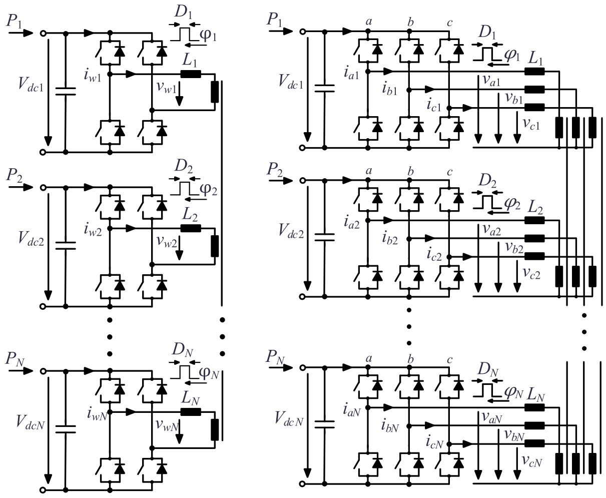


(a) (b)

Fig. 1. Circuit diagrams of MAB converters: (a) single-phase configuration and (b) three-phase configuration.

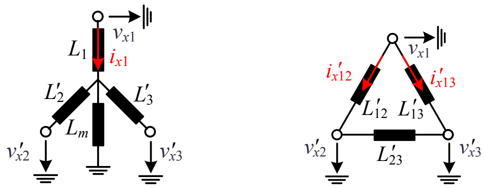


(a) (b)

Fig. 2. Exemplary equivalent circuits for both single-phase and three-phase MAB converters: (a) star circuit and (b) mesh circuit.

to three-phase MAB. Therefore, through flux domain analysis, this work identifies the limitations of these conditions for three phase configuration and adapts them for three-phase MABs. Based on the extended soft-switching constraints, modulation design of three-phase MABs can be simplified.

## II. Fundamental Background of MAB Converters

The MAB converters consist of a multi-winding transformer connected to active bridges, as illustrated in Fig. 2. Their single-phase and three-phase configurations are shown in Fig. 2(a) and (b), respectively. Regardless of the phase number, an $N$-port MAB can change $N$ duty cycles and $(N-1)$ port-to-port load angles. Since the total power sum of all ports is zero, the number of power conditions for the desired power flow is $(N-1)$. Therefore, under multi-variable modulation, there are $N$ residual degrees of freedom while satisfying the $(N-1)$ power conditions. These residual degrees of freedom can be utilized to minimize an arbitrary loss objective, such as conduction, switching, or total losses.

To minimize the loss objective, the candidate domain consisting of $N$ duty cycles should be investigated. However, the size of the candidate domain exponentially increases with $N$ and this broad space can require significant time to find the optimal solution. In this case, for a single-phase MAB, the sufficient conditions for soft-switching can be utilized [23], [24]:

$$D_1 V_{dc1} = D_2 V'_{dc2} = \cdots = D_N V'_{dcN}. \tag{1}$$

Here, $D_n$ and $V_{dcn}$ represent the duty cycle and dc voltage of an arbitrary $n$-port, and $'$ stands for the equivalent conversion into the first port reference.

Since the number of equality conditions is $(N-1)$, the residual degrees of freedom can be reduced to unity from $N$ by using these sufficient conditions. As soft switching is guaranteed through these equations, this unique degree of freedom can be utilized to minimize the conduction loss or both conduction and switching losses over the compressed candidate domain.

To assess power and loss depending on the selected duty cycles, equivalent models of MABs are needed. Representative equivalent models, star and mesh circuits, are illustrated in Fig. 2. While single-phase and three-phase MABs share common equivalent model structures as in this figure, the difference is whether the state variables are scalar or a 2-dimensional vector. The star circuit in Fig.2(a) represents the physical structure of the multi-winding transformer, comprising the common magnetizing branch and the other leakage branches.

In contrast, the mesh circuit in Fig. 2(b) is a physically-irrelevant model derived from the star circuit using the star-mesh conversion [25]. Since each node current independent of the others, it is simpler to calculate them. Based on the superposition of node currents in the mesh circuit, each port current in star circuits can be calculated.

## III. Extension of Soft-Switching Constraints for Three-Phase MAB Converters

The differences between single-phase and three-phase MAB converters primarily stem from the voltage patterns that depend on the duty cycles. The voltage outputs of the single-phase active bridge are one-dimensional, as illustrated in Fig. 3(a). Consequently, the single-phase active bridge exhibits a straightforward voltage pattern according to the duty cycle, as illustrated in Fig. 3(b).

In contrast, the voltage outputs of the three-phase active bridge are two-dimensional in the stationary $\alpha$-$\beta$ plane, as illustrated in Fig. 4(a). Subsequently, according to the duty cycle of the active bridge, their sequences are changed, as illustrated in Fig.4. The voltage patterns with duty-cycles, which are less than 1/3, between 1/3 and 1/2, and equal to 1/2, are shown in Fig. 4(b), (c), and (d), respectively.

Considering all voltage patterns applied to the mesh circuit, deriving current profiles to assess the soft-switching constraints in (1) is significantly complex. Therefore, this article proposes an intuitive geometric analysis method in the flux-domain to assess soft-switching. Assuming negligible winding resistance, the port flux-linkages, $\lambda'_{xj}$, are defined as the time integral of the corresponding port voltage, $v'_{xj}$ as follows:

$$\lambda'_{xj} = \int v'_{xj} dt, x \in \{w, \alpha\beta\}. \tag{2}$$

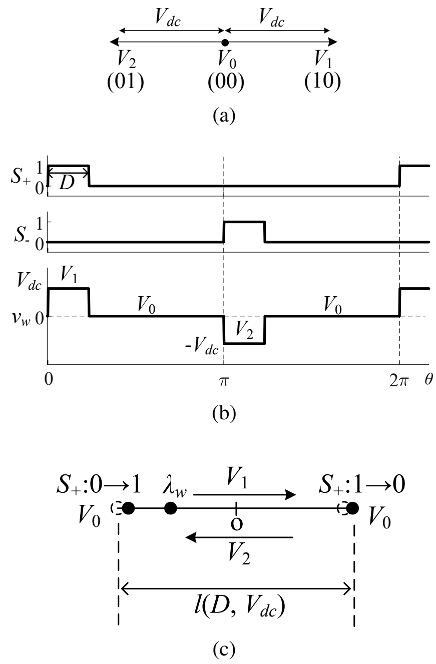


Fig. 3. (a) Voltage output vectors of each single-phase active bridge, (b) the voltage sequences according to the duty cycle, $0 < D < \frac{1}{2}$, and (c) the corresponding port flux trajectory.

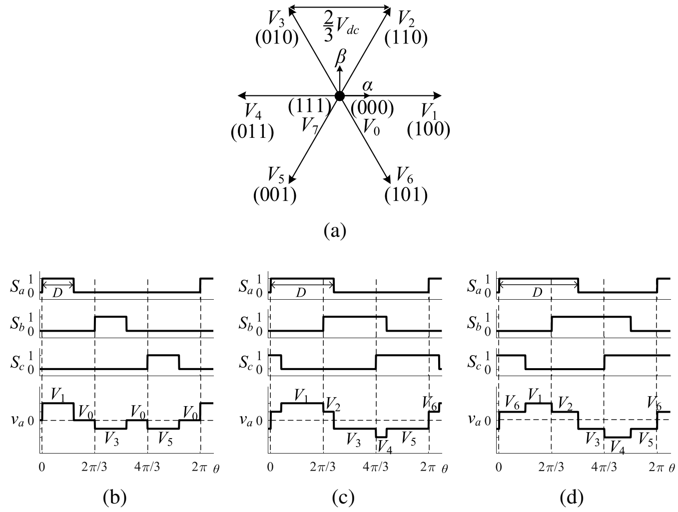


Fig. 4. (a) Voltage output vectors of each three-phase active bridge and voltage sequences according to the duty cycle: (b) $0 < D < \frac{1}{3}$, (c) $\frac{1}{3} < D < \frac{1}{2}$, and (d) $D = \frac{1}{2}$.

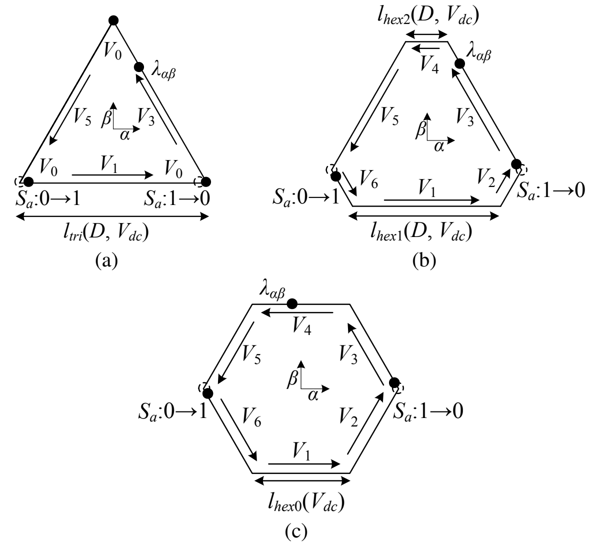


Fig. 5. Port flux-linkage trajectories according to the duty cycle: (a) $0 < D < \frac{1}{3}$, (b) $\frac{1}{3} < D < \frac{1}{2}$, and (c) $D = \frac{1}{2}$.

In this equation, the subscript $w$ represents the one-dimensional variables for the single-phase configuration, and the subscript $\alpha\beta$ denotes the two-dimensional variables for the three-phase configuration.

As illustrated in Fig. 2, the $j$-th port current in the star circuit, $i'_{xj}$ is expressed in terms of the current flowing to adjacent ports in the mesh circuit as follows:

$$i'_{xj} = \sum_{k=1,k\neq j}^{N} i'_{xjk}, x \in \{w, \alpha\beta\}. \quad (3)$$

The currents in the mesh circuit can be derived in terms of the port-flux linkages as:

$$\begin{aligned} i'_{xjk} &= \frac{1}{L'_{jk}} \int (v'_{xj} - v'_{xk}) dt \\ &= \frac{\lambda'_{\alpha\beta j} - \lambda'_{\alpha\beta k}}{L'_{jk}}, x \in \{w, \alpha\beta\}. \end{aligned} \quad (4)$$

By substituting (4) into (3), the port current is given by:

$$i'_{xj} = \sum_{k=1,k\neq j}^{N} \frac{\lambda'_{xj} - \lambda'_{xk}}{L'_{jk}}, x \in \{w, \alpha\beta\}. \quad (5)$$

Consequently, the port currents of the MAB converters are expressed by the differences between port flux-linkages. Therefore, for both single-phase and three-phase MAB converters, the current profiles can be straightforwardly assessed through the geometric relationship among the port flux-linkages.

The steady-state trajectory of the port flux-linkages can be derived from the time integral of the voltage sequences. For the single-phase configuration, the port flux-linkage spans a one-dimensional trajectory regardless of the duty cycle, as depicted in Fig. 3(c). In contrast, that in the three-phase configuration spans two-dimensional trajectories depending on the duty cycle, as shown in Fig. 5. The steady-state flux trajectory becomes a regular triangle for a duty cycle less than 1/3, an asymmetric hexagon for a duty cycle between 1/3 and 1/2, and a regular hexagon for a duty cycle of 1/2.

Note that regardless of the phase configuration or the trajectory type, the port flux-linkage is situated at the vertices at the switching instants. For the single-phase configuration, the port flux-linkage leaves or reaches a vertex, when the top switch at the positive pole turns on or off, respectively, as illustrated in

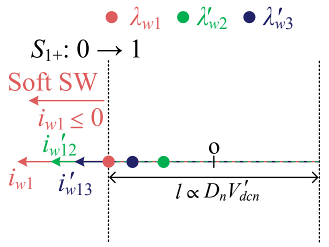


Fig. 6. Port flux-linkage trajectories of the single-phase MAB converter under the original soft-switching constraints.

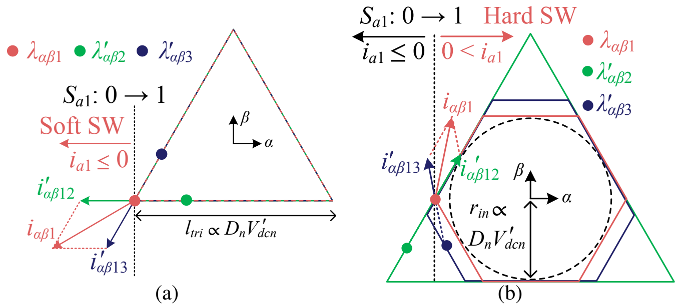


Fig. 7. Port flux-linkage trajectories of the three-phase MAB converter under the original soft-switching constraints (a) with the maximum duty cycle less than 1/3 and (b) with the maximum duty cycle greater than 1/3.

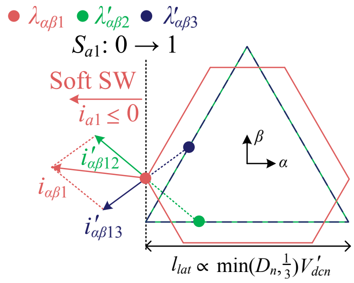


Fig. 8. Port flux-linkage trajectories under the extended soft-switching constraints with the maximum duty cycle greater than 1/3 .

Fig. 3(c). For the three-phase configuration, when the $a$-phase top switch turns on, the port flux-linkage leaves from a vertex, and it reaches a vertex when the corresponding switch turns off, as illustrated in Fig 5. Therefore, by investigating the port current when the port flux-linkage is situated at a vertex, the current polarity for soft-switching can be identified.

When the original soft-switching constraints in (1) are applied to the single-phase MAB converter, the port flux trajectories are illustrated as in Fig. 6 . Since the widths of the line trajectories are proportional to the product of $D_n$ and $V'_{dcn}$, all trajectories overlap. Consequently, the flux-linkage positions cannot induce the current polarity that causes hard switching, thereby guaranteeing soft-switching. For instance, when the port 1 flux is located at the left vertex, the other port flux-linkages cannot lie further to the left, resulting only in individual flux-difference directions that align with the current polarity for soft-switching.

For the three-phase configuration, the original soft-switching constraints are applied, as illustrated in Fig. 7 . When the duty cycles of all ports are less than 1/3, all trajectories become regular triangles as depicted in Fig. 7(a). Since the side lengths of the triangular trajectories are proportional to $D_n V'_{dcn}$, all trajectories overlap each other. Likewise, the flux-linkage positions cannot induce the current polarity that causes hard switching, thus guaranteeing soft-switching.

For instance, when the port 1 flux is located at a vertex and the corresponding $a$-phase top-switch turns on, hard switching occurs if the current polarity is positive. Since all other flux - linkages lie on the right side of port 1 flux-linkage, all current components induced from the flux-linkage differences have non-positive $a$-phase currents. Therefore, the port 1 current as a superposition of these individual current components also has a non-positive $a$-phase current, guaranteeing soft-switching of the corresponding switch.

In contrast, when the maximum duty cycle is greater than 1/3, the trajectories no longer overlap as regular triangles. In this case, their inscribed circles overlap instead, since their radii are proportional to $D_n V'_{dcn}$. However, in this case, flux-linkage positions inducing hard switching can exist, and therefore soft-switching is not guaranteed.

To guarantee soft-switching of three-phase MAB even with the maximum duty cycle greater than 1/3, the sufficient conditions are extended by utilizing the geometric features of the port flux-linkages, as follows:

$$\begin{aligned} \min\left(\frac{1}{3}, D_1\right) V_{dc1} &= \min\left(\frac{1}{3}, D_2\right) V'_{dc2} \\ &= \ldots = \min\left(\frac{1}{3}, D_N\right) V'_{dcN}. \end{aligned} \tag{6}$$

The port flux-linkage trajectories under these extended soft-switching constraints are depicted as in Fig. 8. Regardless of the duty cycle, the lateral width is proportional to $\min\left(\frac{1}{3}, D_n\right) V'_{dcn}$, leading to matched widths under these extended constraints. Therefore, the differences between port-flux linkages only induce the individual current components that trigger soft-switching. Consequently, all port currents, as superpositions of these individual components, have the current polarity required for soft-switching, even when the maximum duty cycle is greater than 1/3.

## IV. Experimental Validation

To validate the extended soft-switching constraints for the three-phase MAB converter, experimental tests were conducted using a prototype three-phase triple-active bridge converter, as illustrated in Fig. 9. The dc voltages of ports 1, 2, and 3 were set to 160 V, 240 V, and 400 V, respectively, and the corresponding turn ratio was 1:1:2. Depending on the dc voltages converted in the port 1 reference, the duty cycles were set following the extended soft-switching constraints in (6).

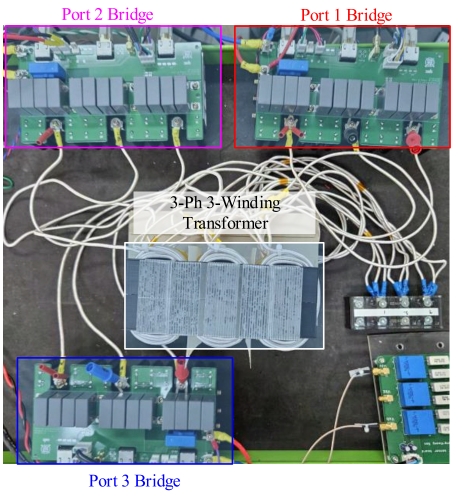


Fig. 9. Experimental setup with the three-phase triple-active bridge converter.

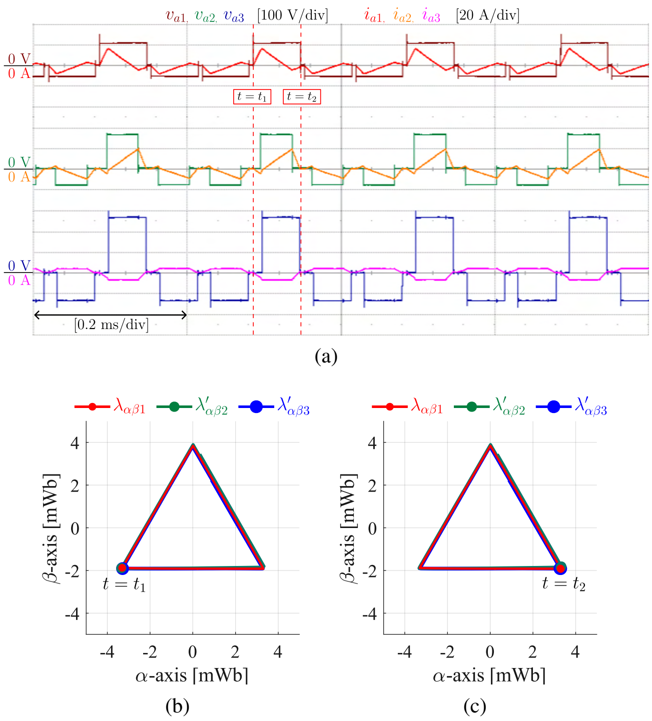


Fig. 10. Switching patterns with the maximum duty cycle less than 1/3 under the extended soft-switching constraints: (a) applied voltage patterns and port currents, and (b) the corresponding flux-linkage trajectories in the $\alpha$-$\beta$ frame.

The case with the maximum duty cycle less than 1/3 was examined, as shown in Fig. 10. The duty cycles, $(D_1, D_2, D_3)$ were set to (0.306, 0.254, 0.206), resulting in an overlap of triangular trajectories. Due to this overlap, all ports achieved soft-switching, as shown in Fig. 10 (a). Port 1 achieved zero-current switching (ZCS) at both rising and falling edges of the voltage pattern, while port 2 achieved zero-voltage switching (ZVS) at both edges. Port 3 achieved ZVS at the rising edge and ZCS at the falling edge. The ZCS in port 1 can also be identified in the flux-domain, as shown in Fig. 10 (b) and (c). Since the other flux-linkages remain at vertices when the port 1 flux-linkage leaves and reaches the vertices, the flux-linkage differences result in zero current at the switching instants.

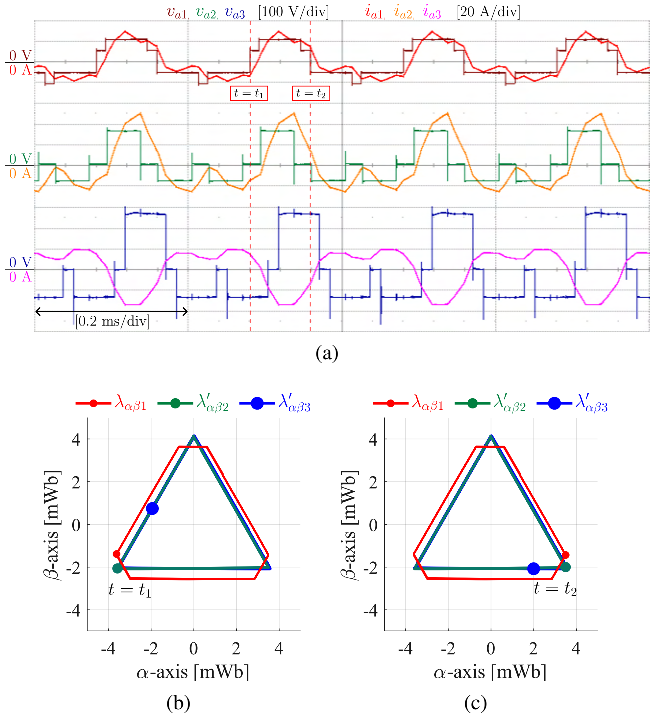


Fig. 11. Switching patterns with the maximum duty cycle greater than 1/3 under the extended soft-switching constraints: (a) applied voltage patterns and port currents, and (b) the corresponding flux-linkage trajectories in the $\alpha$-$\beta$ frame.

The other case with the maximum duty cycle greater than 1/3 was investigated, as shown in Fig. 11. $(D_1, D_2, D_3)$ were set to (0.394, 0.22, 0.264) to match the lateral width of the port flux-linkage trajectories. Due to this width matching, all ports achieved soft-switching, as shown in Fig. 11(a). All ports achieved ZVS at both rising and falling edges of their voltage pattern. The ZVS of port 1 can also be identified in Fig. 11(b) and (c). Since one of the other port flux-linkage remains at the sides when the port 1 flux-linkage leave and reach the vertices, the flux-linkage differences result in the current polarities required for ZVS. Overall, the extended soft-switching constraints guaranteed soft-switching of the three-phase MAB converter even with the maximum duty cycle greater than 1/3.

## V. Conclusion

This work proposed the extended soft-switching constraints to simplify the modulation design of three-phase MAB converters. For this extension, a geometric analysis method using port flux-linkages was presented. Through this flux-domain analysis, the effectiveness and limitations of the original soft-switching constraints for single-phase MABs were investigated for their application to three-phase MABs. To guarantee soft-switching when the maximum duty cycle is greater than 1/3, the extended soft-switching constraints were derived using the flux-domain analysis. The validity of the extended soft-switching constraints was demonstrated through experimental tests.

## References


[1] C. Zhao, S. D. Round, and J. W. Kolar, "An isolated three-port bidirectional dc-dc converter with decoupled power flow management," *IEEE transactions on power electronics*, vol. 23, no. 5, pp. 2443–2453, 2008.

[2] M. Neubert, A. Gorodnichev, J. Gottschlich, and R. W. De Doncker, "Performance analysis of a triple-active bridge converter for interconnection of future dc-grids," in *2016 IEEE Energy Conversion Congress and Exposition (ECCE)*. IEEE, 2016, pp. 1–8.

[3] G. Buticchi, L. F. Costa, D. Barater, M. Liserre, and E. D. Amarillo, "A quadruple active bridge converter for the storage integration on the more electric aircraft," *IEEE Transactions on Power Electronics*, vol. 33, no. 9, pp. 8174–8186, 2017.

[4] L. F. Costa, G. Buticchi, and M. Liserre, "Optimum design of a multiple-active-bridge dc–dc converter for smart transformer," *IEEE Transactions on Power Electronics*, vol. 33, no. 12, pp. 10 112–10 121, 2018.

[5] Y. Chen, P. Wang, H. Li, and M. Chen, "Power flow control in multi-active-bridge converters: Theories and applications," in *2019 IEEE Applied Power Electronics Conference and Exposition (APEC)*. IEEE, 2019, pp. 1500–1507.

[6] J. Lee, J. Yun, H. Kim, and S. Cui, "High-fidelity fea-based circuit simulation for multi-active bridge converter," in *2024 IEEE Energy Conversion Congress and Exposition (ECCE)*. IEEE, 2024, pp. 3765–3770.

[7] N. Soltau, H. A. B. Siddique, and R. W. De Doncker, "Comprehensive modeling and control strategies for a three-phase dual-active bridge," in *2012 International Conference on Renewable Energy Research and Applications (ICRERA)*. IEEE, 2012, pp. 1–6.

[8] N. H. Baars, J. Everts, C. G. Wijnands, and E. A. Lomonova, "Performance evaluation of a three-phase dual active bridge dc–dc converter with different transformer winding configurations," *IEEE Transactions on Power Electronics*, vol. 31, no. 10, pp. 6814–6823, 2015.

[9] J. Yun and S. Cui, "Enhanced active thermal balancing strategy for three-phase dual-active bridge converter suppressing transformer flux saturation," *IEEE Transactions on Power Electronics*, 2024.

[10] J. Yun, S. Cui, and S.-K. Sul, "Instantaneous pulse pattern control for optimized dynamic performance of three-phase dual-active bridge converter," *IEEE Transactions on Power Electronics*, 2025.

[11] M. Neubert, S. P. Engel, J. Gottschlich, and R. W. De Doncker, "Dynamic power control of three-phase multiport active bridge dc-dc converters for interconnection of future dc-grids," in *2017 IEEE 12th International Conference on Power Electronics and Drive Systems (PEDS)*. IEEE, 2017, pp. 639–646.

[12] M. Neubert, H. van Hoek, J. Gottschlich, and R. W. De Doncker, "Soft-switching operation strategy for three-phase multiport-active bridge dc-dc converters," in *2017 IEEE 12th International Conference on Power Electronics and Drive Systems (PEDS)*. IEEE, 2017, pp. 1–207.

[13] J. Yun, J. Lee, G. De Carne, and S. Cui, "Instantaneous pulse pattern control of three-phase multi-active bridge dc-dc converters," *IEEE Transactions on Power Electronics*, 2026.

[14] P. Koohi, A. J. Watson, J. C. Clare, T. B. Soeiro, and P. W. Wheeler, "A survey on multi-active bridge dc-dc converters: Power flow decoupling techniques, applications, and challenges," *Energies*, vol. 16, no. 16, p. 5927, 2023.

[15] M. Liao, H. Li, P. Wang, T. Sen, Y. Chen, and M. Chen, "Machine learning methods for feedforward power flow control of multi-active-bridge converters," *IEEE Transactions on Power Electronics*, vol. 38, no. 2, pp. 1692–1707, 2022.

[16] A. Thönnessen, C. Fronczek, and R. W. De Doncker, "Instantaneous flux and current control for three-phase multi-active-bridge dc-dc converters," in *2023 25th European Conference on Power Electronics and Applications (EPE'23 ECCE Europe)*. IEEE, 2023, pp. 1–8.

[17] R. Yapa and A. Forsyth, "Extended soft switching operation of the triple active bridge converter," in *6th IET International Conference on Power Electronics, Machines and Drives (PEMD 2012)*. IET, 2012, pp. 1–6.

[18] J. Li, Q. Luo, T. Luo, D. Mou, and M. Liserre, "Efficiency optimization scheme for isolated triple active bridge dc–dc converter with full soft-switching and minimized rms current," *IEEE Transactions on Power Electronics*, vol. 37, no. 8, pp. 9114–9128, 2022.

[19] S. Dey and A. Mallik, "Multivariable-modulation-based conduction loss minimization in a triple-active-bridge converter," *IEEE Transactions on Power Electronics*, vol. 37, no. 6, pp. 6599–6612, 2022.

[20] A. A. Ibrahim, A. Zilio, T. Younis, D. Biadene, T. Caldognetto, and P. Mattavelli, "Optimal modulation of triple active bridge converters by an artificial-neural-network approach," *IEEE Transactions on Industrial Electronics*, vol. 71, no. 3, pp. 2590–2600, 2023.

[21] C. Gao, K. Li, Z. Zhang, S. Zhang, S. Zhang, X. You, and S. Lu, "Generalized model of n-port modular multi-active-bridge converter with multiple-phase-shift modulation," *IEEE Transactions on Transportation Electrification*, 2024.

[22] A. Thönnessen, C. Fronczek, and R. W. De Doncker, "Duty-cycle control of three-phase multi-active-bridge converters," *IEEE Journal of Emerging and Selected Topics in Power Electronics*, 2025.

[23] H. Tao, A. Kotsopoulos, J. L. Duarte, and M. A. Hendrix, "Transformer-coupled multiport zvs bidirectional dc–dc converter with wide input range," *IEEE transactions on power electronics*, vol. 23, no. 2, pp. 771–781, 2008.

[24] M. Neubert, "Modeling, synthesis and operation of multiport-active bridge converters," Ph.D. dissertation, Dissertation, Rheinisch-Westfälische Technische Hochschule Aachen, 2020, 2020.

[25] E. Wilkinson, "Mesh/star and star/mesh conversions," *IEEE Transactions on Education*, vol. 10, no. 2, pp. 103–105, 2007.